Non-fibrillar oligomeric amyloid- within synapses

Non-fibrillar oligomeric amyloid-β within synapses

Eleanor K. Pickett[a], Robert M. Koffie[b], Susanne Wegmann[b], Christopher M. Henstridge[a], Abigail G. Herrmann[a], Marti Colom-Cadena[c], Alberto Lleo[c], Kevin R. Kay[b], Melissa Vaught[b], Roy Soberman[b], Dominic M. Walsh[d], Bradley T. Hyman[b], and Tara L. Spires-Jones[a]*

[a]The University of Edinburgh Centre for Cognitive and Neural Systems, Centre for Dementia Prevention and the Euan MacDonald Centre for Motor Neurone Disease Research, 1 George Square, Edinburgh, UK

[b]Massachusetts General Hospital and Harvard Medical School, 114 16th Street, Charlestown, MA 02129, USA

[c]Department of Neurology, Institut d'Investigacions Biomèdiques Sant Pau - Hospital de Sant Pau, Universitat Autònoma de Barcelona, Barcelona, Spain. Centro de Investigación Biomédica en Red en Enfermedades Neurodegenerativas, CIBERNED, Spain

[d]Laboratory for Neurodegenerative Research, Center for Neurologic Diseases, Brigham and Women's Hospital and Harvard Medical School, Harvard Institutes of Medicine, Boston, MA 02115, USA

Running title: Characterizing synaptic Aβ

Manuscript accepted for publication in the Journal of Alzheimer's Disease 18 April 2016
http://www.j-alz.com

*Corresponding Author:
Tara L. Spires-Jones, D. Phil
Centre for Cognitive and Neural Systems
1 George Square
Edinburgh EH8 9JZ UK
Phone: +44(0) 131 651 1895 Fax: +44(0) 131 651 1832
Tara.Spires-Jones@ed.ac.uk

Abstract

Alzheimer's disease (AD) is characterized by memory loss, insidious cognitive decline, profound neurodegeneration and the extracellular accumulation of amyloid-beta (Aβ) peptide in senile plaques and intracellular accumulation of tau in neurofibrillary tangles. Loss and dysfunction of synapses are believed to underlie the devastating cognitive decline in AD. A large amount of evidence suggests that oligomeric forms of Aβ associated with senile plaques are toxic to synapses, but the precise sub-synaptic localization of Aβ and which forms are synaptotoxic remain unknown. Here, we characterize the sub-synaptic localization of Aβ oligomers using three high-resolution imaging techniques, stochastic optical reconstruction microscopy, immunogold electron microscopy and Förster resonance energy transfer in a plaque-bearing mouse model of Alzheimer's disease. With all three techniques, we observe oligomeric Aβ inside synaptic terminals. Further, we tested a panel of Aβ antibodies using the relatively high-throughput array tomography technique to determine which forms are present in synapses. Our results show that different oligomeric Aβ species are present in synapses and highlight the potential of array tomography for rapid testing of aggregation state specific Aβ antibodies in brain tissue.

Key Words

Alzheimer's Disease

Amyloid-β

Synapses

Array Tomography

Introduction

Alzheimer's disease (AD) is a devastating neurodegenerative disease associated with profound cognitive decline and memory dysfunction. Pathologically, the brains of patients are characterized by the presence of aggregated amyloid-beta (Aβ) in senile plaques, the intracellular accumulation of hyperphosphorylated tau in neurofibrillary tangles, and brain atrophy due to loss of neurons and synapses [1]. Of these pathological changes in AD brain, decreased connectivity between neurons due to synapse loss correlates most strongly with cognitive decline.

A large body of evidence supports a role for soluble amyloid-beta (Aβ) in synapse dysfunction and collapse [2-6]. Aβ, particularly in oligomeric form, facilitates long-term depression and inhibits long-term potentiation, both electrophysiological correlates of memory formation [7-9]. Whether Aβ induces synapse loss directly by interaction with synaptic receptors or indirectly through interactions with intermediate molecules is not clear, it is therefore necessary to study these interactions at the synaptic level. However, synapses are too small to be visualized accurately using traditional light microscopy (including multiphoton and confocal imaging) due to the limitation of the axial (z) resolution. The array tomography technique developed by Micheva and Smith [10, 11] overcomes the *z* resolution limit by physically cutting fixed tissue samples into 70 nm serial sections. This enables the visualization of synapses and proteins of interest using standard immunofluorescence techniques. Using the oligomer-recognizing Aβ antibody NAB61 [12] on tissue prepared for array tomography, we previously demonstrated that oligomeric Aβ (oAβ) accumulates in a halo around the edges of plaques and colocalizes with a subset of synapses in wild-type and APPswe/PS1deltaE9 mice [13]. We further pioneered the use of array tomography for human postmortem tissue [14] and found that in human AD brain,

oAβ is associated with a subset of small synapses near plaques, confirming the relevance of this pathway to human disease [15].

Since the association of oAβ with synapses occurs most often in the halo of oligomers surrounding plaques, we assume that the synaptic oAβ derives from extracellular sources and binds to receptors in the synaptic cleft. Thus we expected that oAβ would bind the extracellular face of the pre and postsynaptic terminals, although data have been presented indicating that oAβ can enter cells through several mechanisms including direct permeabilization of the membrane by oAβ [16] and endocytosis [17]. The resolution of array tomography imaged with standard fluorescent microscopy is approximately 250 nm in the x-y plane, which does not allow accurate determination of whether oAβ is found in the synaptic cleft or within synapses with standard imaging techniques. Here we have examined whether NAB61-positive Aβ oligomers are found in the synaptic cleft or within the postsynapse using three high resolution imaging techniques: stochastic optical reconstruction microscopy (STORM), immunogold transmission electron microscopy (TEM), combined array tomography and Förster resonance energy transfer (FRET) imaging. All of these techniques indicate that oAβ is present within the postsynapse and further validate the use of array tomography for accurate localization of pathological proteins with synapses.

Following the validation of the array tomography technique for accurate colocalization of oAβ at synapses, we tested a panel of Aβ antibodies: the previously characterized monoclonal aggregate-preferring oAβ antibody (NAB61) which recognizes oligomers and fibrils but not monomers [12], a monoclonal aggregate-selective antibody (1C22) [18], a conformation-specific antibody known to detect fibrillar oAβ arranged in in-register parallel β sheets (OC) [19-21] and a polyclonal anti-Aβ antibody (AW7) which recognises multiple Aβ assemblies and epitopes,

including monomeric Aβ40 and Aβ42 [22]. We explore to what extent these antibodies bind oAβ and recognise synapse-associated oAβ. Applying this array tomography approach in a transgenic AD mouse model (APP/PS1), we demonstrate that all four Aβ antibodies co-localize with a subset of postsynaptic densities and a subset of presynapses around plaques in APP/PS1 brain.

This study illustrates the power of array tomography for detecting pathological protein conformations at individual synapses, and confirms with multiple antibody probes that oAβ is present in synapses in a mouse model of AD.

Material and Methods

Animals

Brains from APP/PS1 (n=9) and wild-type (n=4) mice aged 8-12 months were used in this study. At this age, APP/PS1 mice have discernible deficits in spatial reference memory [23], substantial plaque pathology and well-established plaque associated synapse loss and synaptic Aβ accumulation [13, 24]. All animal experiments were performed in accordance with institutional and national ethics guidelines and approved by the Harvard Medical School Institutional Animal Care and Use Committee and the UK Home Office.

STORM

Ultra-thin sections (70 nm) of APP/PS1 mouse brains were prepared from array tomography-embedded blocks as described below. Slides were incubated in fresh 0.1% (w/v) sodium borohydride (NaBH4) in PBS for 7 minutes to quench autofluorescence, blocked in 5% goat serum in PBS for 30 minutes, immunolabeled for PSD and oAβ (Table 1), and then post-fixed with 3% paraformaldehyde and 0.1% glutaraledehyde in PBS. Immunolabeling was done using

goat anti-PSD95 and then donkey anti-goat Alexa488 and for oAβ using NAB61 (dilution 1:20) and then 3 mg/ml goat anti-mouse antibody (Jackson) labeled with a Cy3 (activator dye)/Alexa647 (reporter dye) photo-switch dye pair for STORM (labeling ratios [antibody:activator:reporter] were [1:1.8:3.7]). Conventional fluorescence imaging of PSD95-Alexa488 and NAB61-Cy3 allowed initial localization of synaptic terminals and amyloid plaques. After bleaching autofluorescence of the tissue with epifluorescent light for 5 minutes, subsequent STORM imaging of NAB61-Cy3-Alexa647 revealed the precise localization of oAβ. STORM imaging buffer (10 mM Tris-HCl pH8.0, 10 mM NaCl, 10% sucrose) contained 1% 2-Mercaptoethanol (Sigma), 34 mg/ml catalase, and 700 mg/ml sucrose oxidase to prevent dye bleaching and enable efficient photo-switching between bright and dark state of the reporter dye.

STORM data acquisition was performed with a 100x oil immersion objective (Plan Apo VC 100x 1.4 oil) using a N-STORM microscope system (Nikon) equipped with perfect focus system, TIRF laser line for plane illumination, and an EM-CCD camera. To reduce the out-of-focus fluorescence, samples were first illuminated with 647 nm imaging laser at low intensity (laser power 1.5 mW), actual imaging cycles contained one frame of 561 nm activation laser (laser power ~0.03 mW) to activate a small fraction of reporter fluorophores followed by 3 frames of 647 nm imaging laser illumination (laser power ~150 mW). A total of 15000 frames were collected at 33 frames per second. STORM data was analyzed with ElementsV (Nikon) applying drift compensation, and allowing for a signal duration of 30 ms and a minimum of 500 photons counted per pixel (camera sensitivity = 0.18 photons per count).

Immunogold-TEM

Four APP/PS1 mice were perfused with PBS containing 4% paraformaldehyde and 0.1% glutaraldehyde, then their brains were dissected and stored in the same buffer at 4°C for 48

hours to complete fixation. 100 μm thick vibratome sections were prepared from these brains and cut into small blocks containing sensory cortex. Tissue blocks were post-fixed in 0.1% osmium tetroxide for 1 hour, then dehydrated through a series of graded ethanols, transferred into propylene oxide, and embedded in araldite/DDSA (dodecyl succinic anhydride) resin with benzyldimethylamine (BDMA) catalyst according to manufacturer instructions (Electron Microscopy Sciences EMS, Hatfield PA USA). 70 nm thick sections were cut on a Leica Ultracut microtome and floated onto formvar carbon-coated nickel EM grids (EMS). Sections were treated with saturated sodium metaperiodate in water for 1 minute to remove excess osmium, and treated for 5 minutes with 1% sodium borohydride and rinsed with 50 mM glycine in PBS to reduce free aldehyde groups. EM grids were incubated in blocking buffer for donkey secondary antibodies (Aurion, EMS) for 30 minutes, then in PBS containing 0.2% BSA and primary antibody NAB61 (Table 1) in a 1:20 dilution for 2 hours at room temperature. Grids were washed in PBS for 5 minutes 6-times and then incubated in PBS containing 0.2% BSA and immunogold-conjugated donkey anti-mouse 15 nm gold conjugate (dilution 1:50, EMS) for 1.5 hours. Sections were washed in PBS as before, post-fixed in PBS containing 2.5% glutaraldehyde, and counter stained with 3% uranyl acetate in 50% ethanol for 15 minutes followed by 4% lead citrate in a CO_2 free environment for 2.5 minutes. EM grids were imaged using a JEOL JEM-1011 transmission electron microscope with Hamamatsu ORCA digital camera (courtesy Marian DiFiglia and the Philly Dake Electron microscopy core). Synapses were defined by an electron dense postsynaptic density adjacent to a presynaptic terminal containing at least 3 synaptic vesicles. Apposition length was measured along the distance of the PSD facing the synaptic cleft of type 1 (putative excitatory) synapses.

FRET microscopy

For acceptor photobleaching FRET analysis [25] of NAB61 and postsynaptic marker PSD95 colocalization, array ribbons from APP/PS1 (n=5) and wild-type (n=4) mice were

immunofluorescently labeled for oAβ using NAB61 and donkey anti-mouse Cy5 (acceptor secondary antibody) and for PSD using goat anti-PSD95 and rabbit anti-goat Cy3 (donor secondary antibody) as described previously [13, 15]. Briefly, array ribbons were rehydrated for 5 minutes in 50 mM glycine in 1X Tris-buffered saline (TBS) and placed in blocking buffer (0.05% Tween and 0.1% BSA in TBS) for 30 minutes. Ribbons were immunostained with primary antibodies against NAB61 and PSD95 (Table 1) overnight at 4°C. The following day sections were washed five times in TBS before fluorescently labeled secondary antibodies were applied at a 1:50 dilution in blocking buffer for 30 minutes. Sections labeled only with PSD95+Cy3 but no NAB61 were used as negative controls. Sections triple labeled for PSD using goat anti-PSD95 as primary, rabbit anti-goat Cy3 as secondary, and donkey anti-rabbit Cy5 as tertiary antibodies functioned as positive controls. Images were taken with a 63x 1.4NA oil objective at excitation wavelengths of 543 nm and 633 nm (~50% laser power, PMT voltages ~625 V) using a Leica confocal microscope equipped with a FRET module (Leica TCS SL). For each field of view, an initial image of Cy3 and Cy5 (PSD and NAB61) fluorescence was acquired, then the Cy5 acceptor fluorophore was bleached at 100% laser power at 633 nm. After bleaching, a second image of the same sample area was obtained using identical settings as for the image taken before bleaching. For image analysis, regions of interest (ROIs) were drawn around PSD95-positive punctae in the pre-bleach image. FRET efficiency, FRETeff, was calculated from Cy3-donor fluorescence intensity before, Dpre, and after, Dpost, as FRETeff = (Dpost-Dpre)/Dpost for each ROI showing Dpost>Dpre. Synapses were considered NAB61-positive if the Cy5-acceptor fluorescence intensity before bleaching was at least 3-times higher than the Cy5 background fluorescence in the same ROI after bleaching.

Array tomography

Fresh brain tissue samples were collected from APP/PS1 transgenic mice as outlined previously [13, 14]. Briefly, small tissue blocks of four 8-12 month old APP/PS1 mice were fixed in 4%

paraformaldehyde and 2.5% sucrose in 20 mM phosphate buffered saline pH7.4 (PBS) for 3 hours. Samples were then dehydrated through ascending cold graded ethanol and embedded into LR White resin (EMS) which was allowed to polymerize overnight at 53°C. Resin embedded tissue blocks were cut into array ribbons of 70 nm thick sections using an ultracut microtome (Leica) equipped with a Jumbo Histo Diamond Knife (Diatome, Hatfield, PA) and collected onto gelatin coated coverslips.

For immunolabeling of synapses and Aβ on “day 1”, array ribbons were immunostained as described for FRET imaging with primary antibodies against NAB61 and PSD95 (Table 1) and fluorescently labeled secondary antibodies (Table 1). Sections were counterstained with 0.01mg/mL 4’-6-diamidino-2-phenylindole (DAPI). For each area of interest, images were obtained on serial sections using a Zeiss axio Imager Z2 epifluorescent microscope at 63X 1.4NA Plan Apochromat objective with equipped CoolSnap digital camera and AxioImager software with array tomography macros (Carl Zeiss, Ltd, Cambridge UK).

Coverslips were removed from slides and washed. All primary and secondary antibodies were stripped for 15 minutes using stripping buffer (0.2 M NaOH 0.02% SDS in ddH20). The staining protocol was repeated as previously described for “day 1” with primary antibodies against 1C22, OC and PSD95 and appropriate secondary antibodies (Table 1). Images were captured in the same location as the previous day using identifiable marked nuclei. Following “day 2” imaging the ribbons were once again stripped of all antibodies and stained with antibodies against AW7 and Synaptophysin for “day 3” (Table 1). Images were obtained in the same location as both days 1 and 2 using specific nuclei as markers. Images from each set of serial sections across the three days were converted into image stacks and aligned using the Image J plug-in, MultiStackReg (courtesy of Brad Busse and P. Thevenaz, Stanford University) [26]. Cropped regions of interest (10 μm^2) around the plaque were generated. Amyloid-beta image stacks were

then binarised using thresholding algorithms in ImageJ. For synaptic images stacks were binarised using an ImageJ script that combines different thresholding algorithms in order to select both high and low intensity synapses in an automated and unbiased manner. Thresholded images were processed and analysed in MATLAB to remove background noise (objects present in only a single section were removed) and to calculate the colocalization of Aβ with both pre- and post-synapses. The % colocalization for each antibody combination from each mouse was calculated as the sum of the number of colocalization/sum total pre- or post-synapses.

Statistical analyses

FRET: From a total of 3462 NAB61-negative and 105 NAB61-positive synapses across the 9 imaged animals (5x APP/PS1, 4x wild-type mice), the mean FRET efficiencies of NAB61-negative, NAB61-positive, positive control, and negative control synapses were calculated for each animal. Significance of variance between mouse genotypes and between the presence and absence of NAB61 at synapses were tested using two-way ANOVA analysis (with SPSS software, SAS). Data are presented as mean and standard error.

Array Tomography: Data for each colocalization combination between the four mice was not normally distributed so the non-parametric Kruskal-Wallis test was performed with Dunn's post-hoc comparisons (GraphPad Prism 4). All values are reported as median and interquartile range.

Data Sharing:

Upon acceptance, all data used in this manuscript including custom image analysis scripts for ImageJ and MATLAB will be freely shared on the University of Edinburgh Data Repository http://datashare.is.ed.ac.uk.

Results

STORM, TEM and FRET confirm presence of oAβ in the postsynaptic density

We have previously shown that oAβ recognised by NAB61 is associated with synaptic degeneration in the APP/PS1 mouse model and human AD patient brain [13, 15]. Here, we further specified the localization of these oAβ species applying several high-resolution imaging techniques. STORM was used to determine the localization of oAβ with respect to PSDs with nanometer precision on array tomography 70 nm sections. After imaging of immunofluorescently labeled PSD and oAβ in ultra-thin sections with conventional epifluorescence, which allowed the initial localization of synapses and the identification of amyloid plaques in the brain, STORM imaging of NAB61 revealed the precise localization of Aβ oligomers in the neuropil surrounding plaques. Overlaying the NAB61–STORM images with the corresponding PSD95-epifluorescence images showed a clear co-localization of oAβ with a subset of PSDs in APP/PS1 mouse brain (Figure 1A-B).

Immunogold labeling of NAB61 in APP/PS1 brain samples observed with TEM was used to determine further the precise subcellular localization of oAβ. We observe the most robust NAB61 staining in close proximity to plaque fibrils (Figure 1C and Supplemental Figure 1) as expected from the intense plaque labeling with NAB61 in immunofluorescence studies. We also observed NAB61 immunogold labeling in both presynaptic and postsynaptic terminals (Figure 1C) confirming our immunofluorescence data showing NAB61 colocalization with synaptic staining in the neuropil. Notably, in synapses, the oAβ was not associated with fibrils, which are readily recognized by TEM (Figure 1C). None of the synapses observed across 4 mice (regardless of whether they were positive for NAB61) contained fibrils. This provides additional confirmation of the previous NAB61 characterization [12] as recognising oligomeric Aβ in addition to our observed fibril staining. NAB61 staining was not restricted to plaques and

synapses. We also observe staining in cell bodies, dendrites, and mitochondria (Supplemental Figure 2), which supports our array tomography immunofluorescence observations of NAB61 in some neuronal cell bodies and in punctae in the neuropil that are not positive for synaptic markers [13, 15].

To determine whether oAβ is present inside PSDs, as indicated by colocalization with PSD95 punctae in array tomography sections, we performed FRET microscopy on these sections, which allows the detection of two fluorophores in close (<10 nm) proximity. After labeling PSDs with antibody PSD95 and donor fluorophore (Cy3) labeled secondary antibody and labeling oAβ with NAB61 and acceptor fluorophore (Cy5) labeled secondary antibody, we performed confocal microscopy of the brain sections before and after bleaching the acceptor (Figure 2). The average FRET efficiency of NAB61-positive synapses in APP/PS1 mice (5.3%) was approximately 3-fold increased compared to NAB61-negative synapses (1.9% FRET efficiency). Similarly, the rare synapses that were NAB61 positive in wild-type also had increased FRET efficiency with PSD95 (5.2%) compared to NAB61 negative synapses (1.7%). Two way ANOVA analysis reveals a significant increase in FRET efficiency in NAB61 positive synapses ($F=5.6$, $p=0.04$). The FRET efficiency of NAB61-negative synapses was similar to the negative control FRET efficiency in which there was no acceptor fluorophores (2.1%). Positive control labeling of PSD95 with both donor and acceptor fluorophores (with a Cy3 labeled secondary antibody and Cy5 labeled tertiary antibody) had an average FRET efficiency of 25%, which is ceiling for our experiment. No difference in FRET efficiency was detected between synapses of wild-type and APP/PS1 mice (two-way ANOVA $F=0.002$, $p=0.962$). There was no interaction between genotype and NAB61 status ($F=0.002$, $p=0.962$), indicating the labelled fluorophores are within 10 nm and due to the distance added by antibody labelling, we estimate that oAβ is within at most 10-30 nm of PSDs in both genotypes.

Array tomography reveals synaptic staining with several markers of Aβ

To characterize the synaptic profile of four Aβ-specific antibodies; NAB61, 1C22, OC and AW7, we immunolabeled Aβ and synaptic markers in array tomography sections of APP/PS1 mouse brains (n=4 mice) in a three-day imaging protocol (Figure 3). In each experiment, a small extra ribbon of sections was used as a stripping control with no primary antibodies applied on the subsequent day. Applying secondary antibodies after stripping confirmed effective stripping of antibodies on each day of staining (Supplemental Figure 3).

We found that all four antibodies labeled plaques in APP/PS1 brains (Figure 4A-D). To determine whether and to what extent oAβ colocalizes with synapses, we applied combinations of PSD recognizing antibody (PSD95), presynaptic recognizing antibody (synaptophysin) and the different Aβ antibodies (Figure 4 and Figure 5). Across four APP/PS1 mice, subsets of PSD-positive synaptic punctae (n=6,548) colocalized with Aβ labeling by NAB61 (9.8% of synaptic punctae), 1C22 (15.9%), AW7 (17.3%) and OC (24.1%) (Figure 6A). Dunn's post-hoc analysis revealed a significant difference between the percentages of NAB61 positive postsynaptic punctae and OC positive postsynaptic punctae ($p<0.05$). Interestingly, colocalization between two Aβ detecting antibodies and PSD95 was observed in a subset of synapses with the highest % colocalization between AW7 + OC (12.3%) and 1C22 + OC (11.5%) (Figure 6B). Further analysis revealed a subset of postsynapses colocalized with all four antibodies (5.0%). Presynaptic staining revealed a subset of synaptophysin-positive synaptic punctae (n=5,573) colocalized with Aβ stained with NAB61 (8.1% of synaptic punctae), 1C22 (11.6%), AW7 (14.3%) and OC (18.9%) (Figure 6A). Dunn's post-hoc analysis revealed a significant difference between the percentages of NAB61 positive presynaptic punctae and OC positive presynaptic punctae ($p<0.05$). In addition, a subset of presynapses colocalized with two Aβ detecting antibodies with the highest % colocalization observed again between combinations of AW7 +

OC (9.0%) and 1C22 + OC (7.8%) (Figure 6C). A subset of presynapses colocalized with three Aβ detecting antibodies and a smaller subset colocalized with all four antibodies (4.0%). These data show that multiple antibodies confirm the presence of oligomeric Aβ in synapses. Further, each of the Aβ antibodies used recognises different confirmations ranging from monomeric Aβ, fibrillar oligomers and fibrils. Since not all synapses containing Aβ are recognized by all of these antibodies and we do not observe fibrils in synapses by EM, we conclude that there are likely multiple forms of soluble Aβ present in synapses. These data further highlight the utility of this technique for measuring synaptic localization of pathological epitopes of proteins.

Discussion

There is mounting evidence that oAβ plays a key role in synapse dysfunction and loss [27]. Oligomeric Aβ modulates several intracellular pathways including activating caspase-3 and calcineurin at the synapse to ultimately culminate in synaptic failure [28-31]. Synaptic dysfunction may precede cognitive decline in AD by several decades and could potentially be reversible [32]. In this study, we addressed two important remaining questions around oAβ–mediated synapse loss, namely is toxic oAβ located in the synaptic cleft or within presynaptic terminals and postsynaptic densities? And which forms of Aβ are associated with synapses?

Whether toxic Aβ at synapses originates from intracellular or extracellular sources is a hotly debated topic in the field [33-36]. Here we used three high-resolution imaging techniques to examine whether oAβ is present within synaptic terminals or decorating the exterior membrane of pre and postsynapses and find that NAB61 labeled oAβ is present inside synapses. Our data suggest that synaptotoxic oAβ derives from the extracellular plaque halo since localization of Aβ at synapses occurs most often in this region [13, 15], however it appears oAβ is present within

synapses (Figures 1-2). This could occur alongside the internalization of synaptic receptors initiated by oAβ or more directly through the reported pores that Aβ can form in membranes [27, 37]. It is also worth noting, that while we specifically examined synapses in this study, we did observe oAβ in other subcellular compartments by TEM. We observed immunogold labelling associated with ribosomes in neuronal somata and dendrites, cell membrane staining, and mitochondrial staining (Supplemental Figure 2). Mitochondrial staining is particularly interesting in light of the large body of literature supporting a role of oAβ in causing mitochondrial damage [38]

Another contentious and important topic on the road to synapse-directed therapeutics is which specific forms of oAβ are toxic at synapses and therefore which would be the best targets. One recent study in mice classified oligomers in mice as type 1 (A11-immunoreactive, Aβ*56) and type 2 (recognized by OC) and concluded that type 2 oligomers were less toxic because of their containment within plaques [21]. Our data indicate that type 2 oligomers (OC positive) are present in synapses, where they may contribute to toxicity. In line with our observations, OC reactivity correlated with onset and severity of AD in human brain samples [39], and synaptotoxic oligomers of Aβ that interact with PrP and inhibit LTP were also recognised by OC [40].

Previous studies of colocalization of proteins within synapses were hampered by the difficulty of techniques such as immunogold EM, which are very low throughput and only allow one or two proteins of interest to be studied. Here we used the relatively high-throughput array tomography technique [14] which allowed us to examine the colocalization of four antibodies within the same pre and postsynaptic terminals. Array tomography is limited by the reliance on antibody staining of synaptic proteins and threshold-based image analyses, which does not guarantee accurate

identification of synaptic puncta due to a combination of antibody specificity and analysis artifacts; however, a recent study using correlative array tomography and electron microscopy confirmed that ~98% of synapses in CA1 were accurately identified with array tomography staining [41]. This powerful technique will be useful since passive immunization with oAβ-specific antibodies is a promising potential treatment in AD, which could specifically reduce synaptic oAβ and reverse or prevent synapse loss. With multiple oAβ-specific antibodies being developed [42-45], it will be crucial to find effective ways to quickly validate these antibodies in brain tissue, without extensive manipulation of brain samples. Conventional methods such as IP-western blotting and size exclusion chromatography required brain tissue to be homogenized, sonicated, and solubilized with different buffer solutions, making it difficult to ascertain whether such extensive sample manipulation introduces artificial Aβ conformers in the sample.

Interestingly, we observe that the four antibodies tested with array tomography all recognized some synaptic Aβ but not at all of the same synapses. While there was some co-localization of two markers in the same synapses, this was at most half of the synapses that were labeled by only one of the antibodies, and synapses with 3 or all 4 of the markers were rare. Post-hoc statistical comparisons between single, double and triple-labeling combinations indicated significantly fewer multiple stained synapses in many of the staining combinations (data not shown). There are limitations to the array tomography technique in both the staining (antibody penetration and affinity) and image analysis (filtering steps to remove noise) making it likely that we did not detect all of the positive synapses for each marker, however the reduced double and further reduced triple labeling across all combinations of antibodies indicates that there are distinct species of Aβ present at different synapses. We expected that the pan- Aβ antibody AW7 would recognize the most synapses and would usually be present with all of the other markers, but this was not the case. It is possible that the fixation procedure or LR-White resin

embedding may affect the Aβ epitopes recognised by AW7. Alternatively, this could potentially be due to the relatively high affinity for AW7 staining fibrils. All antibodies tested labeled the plaque core to some extent, but AW7 stained fibrils very strongly. We postulate that if the antibodies have a high affinity for fibrils, they may have less opportunity to bind the less abundant synaptic Aβ, and the lower intensity synaptic staining may be below the detection level due to the bright staining of the fibrils in the same microscopic field.

Another important observation in this study is the association of Aβ with both pre and postsynaptic elements. Many of the studies of the synaptic effects of Aβ implicate postsynaptic mechanisms in synapse toxicity, but presynaptic mechanisms have also been found [27, 46]. Our data show more Aβ at excitatory postsynapses than at presynaptic terminals consistent with the ideas that both pre and postsynapses are affected by Aβ and that postsynaptic processes are particularly important in synapse loss. Our data indicate that there is not likely a single synaptotoxic species of Aβ but instead multiple conformers are present inside pre and postsynaptic terminals near plaques. It is clear that Aβ-induced synaptic toxicity plays a major role in the pathogenesis of AD and that targeting synaptic pathology aiming at protecting or reversing synaptic damage is a promising avenue for developing disease-modifying treatments.

Acknowledgments

Funding provided by Alzheimer's Society, Alzheimer's Research UK and the Scottish Government, a University of Edinburgh Wellcome Trust ISSF, Instituto de Salud Carlos III (PI14/01561), "Marató TV3" grants (20142610) and an anonymous foundation. This work was supported by grants to DMW from the National Institutes of Health (AG046275). We would like to thank Virginia Lee for providing NAB61 antibody, Charles Glabe for OC antibody and Marian DiFiglia for access to the Philly Dake Electron Microscopy Core.

References:

[1] Serrano-Pozo A, Frosch MP, Masliah E, Hyman BT (2011) Neuropathological alterations in Alzheimer disease. *Cold Spring Harb Perspect Med* **1**, a006189.

[2] Hardy J, Selkoe DJ (2002) The amyloid hypothesis of Alzheimer's disease: progress and problems on the road to therapeutics. *Science* **297**, 353-356.

[3] Cleary JP, Walsh DM, Hofmeister JJ, Shankar GM, Kuskowski MA, Selkoe DJ, Ashe KH (2005) Natural oligomers of the amyloid-beta protein specifically disrupt cognitive function. *Nat Neurosci* **8**, 79-84.

[4] Knafo S, Gouras GK, Yan XX, Spires-Jones T (2012) Pathology of synapses and dendritic spines. *Neural Plast* **2012**, 972432.

[5] Shankar GM, Bloodgood BL, Townsend M, Walsh DM, Selkoe DJ, Sabatini BL (2007) Natural oligomers of the Alzheimer amyloid-beta protein induce reversible synapse loss by modulating an NMDA-type glutamate receptor-dependent signaling pathway. *J Neurosci* **27**, 2866-2875.

[6] Walsh DM, Klyubin I, Shankar GM, Townsend M, Fadeeva JV, Betts V, Podlisny MB, Cleary JP, Ashe KH, Rowan MJ, Selkoe DJ (2005) The role of cell-derived oligomers of Abeta in Alzheimer's disease and avenues for therapeutic intervention. *Biochem Soc Trans* **33**, 1087-1090.

[7] Shankar GM, Li S, Mehta TH, Garcia-Munoz A, Shepardson NE, Smith I, Brett FM, Farrell MA, Rowan MJ, Lemere CA, Regan CM, Walsh DM, Sabatini BL, Selkoe DJ (2008) Amyloid-beta protein dimers isolated directly from Alzheimer's brains impair synaptic plasticity and memory. *Nat Med* **14**, 837-842.

[8] Barry AE, Klyubin I, Mc Donald JM, Mably AJ, Farrell MA, Scott M, Walsh DM, Rowan MJ (2011) Alzheimer's disease brain-derived amyloid-beta-mediated inhibition of LTP in vivo is prevented by immunotargeting cellular prion protein. *J Neurosci* **31**, 7259-7263.

[9] Freir DB, Nicoll AJ, Klyubin I, Panico S, Donald JM, Risse E, Asante EA, Farrow MA, Sessions RB, Saibil HR, Clarke AR, Rowan MJ, Walsh DM, Collinge J (2011) Interaction between prion protein and toxic amyloid β assemblies can be therapeutically targeted at multiple sites. *Nature communications* **2**, 336.

[10] Micheva KD, Busse B, Weiler NC, O'Rourke N, Smith SJ (2010) Single-synapse analysis of a diverse synapse population: proteomic imaging methods and markers. *Neuron* **68**, 639-653.

[11] Micheva KD, Smith SJ (2007) Array tomography: a new tool for imaging the molecular architecture and ultrastructure of neural circuits. *Neuron* **55**, 25-36.

[12] Lee EB, Leng LZ, Zhang B, Kwong L, Trojanowski JQ, Abel T, Lee VM (2006) Targeting amyloid-beta peptide (Abeta) oligomers by passive immunization with a conformation-selective monoclonal antibody improves learning and memory in Abeta precursor protein (APP) transgenic mice. *J Biol Chem* **281**, 4292-4299.

[13] Koffie RM, Meyer-Luehmann M, Hashimoto T, Adams KW, Mielke ML, Garcia-Alloza M, Micheva KD, Smith SJ, Kim ML, Lee VM, Hyman BT, Spires-Jones TL (2009) Oligomeric amyloid beta associates with postsynaptic densities and correlates with excitatory synapse loss near senile plaques. *Proc Natl Acad Sci U S A* **106**, 4012-4017.

[14] Kay KR, Smith C, Wright AK, Serrano-Pozo A, Pooler AM, Koffie R, Bastin ME, Bak TH, Abrahams S, Kopeikina KJ, McGuone D, Frosch MP, Gillingwater TH, Hyman BT, Spires-Jones TL (2013) Studying synapses in human brain with array tomography and electron microscopy. *Nat Protoc* **8**, 1366-1380.

[15] Koffie RM, Hashimoto T, Tai HC, Kay KR, Serrano-Pozo A, Joyner D, Hou S, Kopeikina KJ, Frosch MP, Lee VM, Holtzman DM, Hyman BT, Spires-Jones TL (2012) Apolipoprotein E4 effects in Alzheimer's disease are mediated by synaptotoxic oligomeric amyloid-beta. *Brain* **135**, 2155-2168.

[16] Kayed R, Pensalfini A, Margol L, Sokolov Y, Sarsoza F, Head E, Hall J, Glabe C (2009) Annular protofibrils are a structurally and functionally distinct type of amyloid oligomer. *J Biol Chem* **284**, 4230-4237.

[17] Nath S, Agholme L, Kurudenkandy FR, Granseth B, Marcusson J, Hallbeck M (2012) Spreading of neurodegenerative pathology via neuron-to-neuron transmission of beta-amyloid. *J Neurosci* **32**, 8767-8777.

[18] Yang T, O'Malley TT, Kanmert D, Jerecic J, Zieske LR, Zetterberg H, Hyman BT, Walsh DM, Selkoe DJ (2015) A highly sensitive novel immunoassay specifically detects low levels of soluble Abeta oligomers in human cerebrospinal fluid. *Alzheimers Res Ther* **7**, 14.

[19] Wu JW, Breydo L, Isas JM, Lee J, Kuznetsov YG, Langen R, Glabe C (2010) Fibrillar oligomers nucleate the oligomerization of monomeric amyloid beta but do not seed fibril formation. *J Biol Chem* **285**, 6071-6079.

[20] Kayed R, Head E, Sarsoza F, Saing T, Cotman CW, Necula M, Margol L, Wu J, Breydo L, Thompson JL, Rasool S, Gurlo T, Butler P, Glabe CG (2007) Fibril specific, conformation dependent antibodies recognize a generic epitope common to amyloid fibrils and fibrillar oligomers that is absent in prefibrillar oligomers. *Mol Neurodegener* **2**, 18.

[21] Liu P, Reed MN, Kotilinek LA, Grant MK, Forster CL, Qiang W, Shapiro SL, Reichl JH, Chiang AC, Jankowsky JL, Wilmot CM, Cleary JP, Zahs KR, Ashe KH (2015) Quaternary Structure Defines a Large Class of Amyloid-beta Oligomers Neutralized by Sequestration. *Cell Rep* **11**, 1760-1771.

[22] McDonald JM, Cairns NJ, Taylor-Reinwald L, Holtzman D, Walsh DM (2012) The levels of water-soluble and triton-soluble Abeta are increased in Alzheimer's disease brain. *Brain Res* **1450**, 138-147.

[23] Jankowsky JL, Melnikova T, Fadale DJ, Xu GM, Slunt HH, Gonzales V, Younkin LH, Younkin SG, Borchelt DR, Savonenko AV (2005) Environmental enrichment mitigates cognitive deficits in a mouse model of Alzheimer's disease. *J Neurosci* **25**, 5217-5224.

[24] Garcia-Alloza M, Robbins EM, Zhang-Nunes SX, Purcell SM, Betensky RA, Raju S, Prada C, Greenberg SM, Bacskai BJ, Frosch MP (2006) Characterization of amyloid deposition in the APPswe/PS1dE9 mouse model of Alzheimer disease. *Neurobiol Dis* **24**, 516-524.

[25] Ishikawa-Ankerhold HC, Ankerhold R, Drummen GP (2012) Advanced fluorescence microscopy techniques--FRAP, FLIP, FLAP, FRET and FLIM. *Molecules (Basel, Switzerland)* **17**, 4047-4132.

[26] Thevenaz P, Ruttimann UE, Unser M (1998) A pyramid approach to subpixel registration based on intensity. *IEEE Trans Image Process* **7**, 27-41.

[27] Spires-Jones TL, Hyman BT (2014) The Intersection of Amyloid Beta and Tau at Synapses in Alzheimer's Disease. *Neuron* **82**, 756-771.

[28] Jo J, Whitcomb DJ, Olsen KM, Kerrigan TL, Lo SC, Bru-Mercier G, Dickinson B, Scullion S, Sheng M, Collingridge G, Cho K (2011) Abeta(1-42) inhibition of LTP is mediated by a signaling pathway involving caspase-3, Akt1 and GSK-3beta. *Nat Neurosci* **14**, 545-547.

[29] D'Amelio M, Cavallucci V, Middei S, Marchetti C, Pacioni S, Ferri A, Diamantini A, De Zio D, Carrara P, Battistini L, Moreno S, Bacci A, Ammassari-Teule M, Marie H, Cecconi F (2011) Caspase-3 triggers early synaptic dysfunction in a mouse model of Alzheimer's disease. *Nat Neurosci* **14**, 69-76.

[30] Spires-Jones TL, Kay K, Matsouka R, Rozkalne A, Betensky RA, Hyman BT (2011) Calcineurin inhibition with systemic FK506 treatment increases dendritic branching and dendritic spine density in healthy adult mouse brain. *Neurosci Lett* **487**, 260-263.

[31] Wu HY, Hudry E, Hashimoto T, Kuchibhotla K, Rozkalne A, Fan Z, Spires-Jones T, Xie H, Arbel-Ornath M, Grosskreutz CL, Bacskai BJ, Hyman BT (2010) Amyloid beta induces

the morphological neurodegenerative triad of spine loss, dendritic simplification, and neuritic dystrophies through calcineurin activation. *J Neurosci* **30**, 2636-2649.

[32] Holtzman DM, Morris JC, Goate AM (2011) Alzheimer's disease: the challenge of the second century. *Sci Transl Med* **3**, 77sr71.

[33] Gouras GK, Tampellini D, Takahashi RH, Capetillo-Zarate E (2010) Intraneuronal beta-amyloid accumulation and synapse pathology in Alzheimer's disease. *Acta Neuropathol* **119**, 523-541.

[34] Youmans KL, Tai LM, Kanekiyo T, Stine WB, Jr., Michon SC, Nwabuisi-Heath E, Manelli AM, Fu Y, Riordan S, Eimer WA, Binder L, Bu G, Yu C, Hartley DM, LaDu MJ (2012) Intraneuronal Abeta detection in 5xFAD mice by a new Abeta-specific antibody. *Mol Neurodegener* **7**, 8.

[35] Wirths O, Dins A, Bayer TA (2012) AbetaPP accumulation and/or intraneuronal amyloid-beta accumulation? The 3xTg-AD mouse model revisited. *J Alzheimers Dis* **28**, 897-904.

[36] Iulita MF, Allard S, Richter L, Munter LM, Ducatenzeiler A, Weise C, Do Carmo S, Klein WL, Multhaup G, Cuello AC (2014) Intracellular Abeta pathology and early cognitive impairments in a transgenic rat overexpressing human amyloid precursor protein: a multidimensional study. *Acta Neuropathol Commun* **2**, 61.

[37] Lasagna-Reeves CA, Glabe CG, Kayed R (2011) Amyloid-beta annular protofibrils evade fibrillar fate in Alzheimer disease brain. *J Biol Chem* **286**, 22122-22130.

[38] Morais VA, Strooper DB (2010) Mitochondria dysfunction and neurodegenerative disorders: cause or consequence. *Journal of Alzheimer's Disease* **20**, 255-263.

[39] Tomic J, Pensalfini A, Head E, Glabe C (2009) Soluble fibrillar oligomer levels are elevated in Alzheimer's disease brain and correlate with cognitive dysfunction. *Neurobiology of Disease* **35**, 352-358.

[40] Nicoll AJ, Panico S, Freir DB, Wright D, Terry C, Risse E, Herron CE, O'Malley T, Wadsworth JD, Farrow MA, Walsh DM, Saibil HR, Collinge J (2013) Amyloid-beta

nanotubes are associated with prion protein-dependent synaptotoxicity. *Nat Commun* **4**, 2416.

[41] Bloss EB, Cembrowski MS, Karsh B, Colonell J, Fetter RD, Spruston N (2016) Structured Dendritic Inhibition Supports Branch-Selective Integration in CA1 Pyramidal Cells. *Neuron* **89**, 1016-1030.

[42] Rasool S, Martinez-Coria H, Milton S, Glabe CG (2013) Nonhuman amyloid oligomer epitope reduces Alzheimer's-like neuropathology in 3xTg-AD transgenic mice. *Mol Neurobiol* **48**, 931-940.

[43] Dorostkar MM, Burgold S, Filser S, Barghorn S, Schmidt B, Anumala UR, Hillen H, Klein C, Herms J (2014) Immunotherapy alleviates amyloid-associated synaptic pathology in an Alzheimer's disease mouse model. *Brain* **137**, 3319-3326.

[44] Guerrero-Munoz MJ, Castillo-Carranza DL, Kayed R (2014) Therapeutic approaches against common structural features of toxic oligomers shared by multiple amyloidogenic proteins. *Biochem Pharmacol* **88**, 468-478.

[45] Hillen H, Barghorn S, Striebinger A, Labkovsky B, Muller R, Nimmrich V, Nolte MW, Perez-Cruz C, van der Auwera I, van Leuven F, van Gaalen M, Bespalov AY, Schoemaker H, Sullivan JP, Ebert U (2010) Generation and therapeutic efficacy of highly oligomer-specific beta-amyloid antibodies. *J Neurosci* **30**, 10369-10379.

[46] Rudy CC, Hunsberger HC, Weitzner DS, Reed MN (2015) The role of the tripartite glutamatergic synapse in the pathophysiology of Alzheimer's disease. *Aging and disease* **6**, 131-148.

Table 1: Summary of antibody details for all experimental techniques

Primary antibody	Source	Dilution	Working concentration (mg/ml)	Secondary antibody
FRET				
NAB61	Courtesy V Lee	1:25	0.107	Donkey anti-mouse Cy5 (acceptor)
PSD95	Abcam (ab12093)	1:50	0.020	Donkey anti-goat Alexa Cy3 (donor)
Immunogold TEM				
NAB61	Courtesy V Lee	1:20	0.134	immunogold-conjugated donkey anti-mouse 15nm gold conjugate
STORM				
NAB61	Courtesy V Lee	1:20	0.134	Goat anti-mouse antibody (Jackson) labeled with Cy3 (activator dye)/Alexa647 (reporter dye)
PSD95	Abcam (ab12093)	1:50	0.020	Donkey anti-goat Alexa 488 Invitrogen
Array Tomography				
NAB61	Courtesy V Lee	1:200	0.013	Donkey anti-mouse Alexa594, Invitrogen
1C22	D Walsh	1:25	0.040	Donkey anti-mouse Alexa488, Invitrogen
OC	Courtesy C Glabe	1:50	polyclonal	Donkey anti-rabbit Alexa647, Invitrogen
AW7	D Walsh	1:500	polyclonal	Donkey anti-rabbit Alexa594, Invitrogen
PSD95	Abcam (ab12093)	1:50	0.020	Donkey anti-goat Alexa488 (day1), Alexa 594 (day 2), Invitrogen
Synaptophysin	Abcam (ab8049)	1:25	0.040	Donkey anti-mouse Alexa488, Invitrogen

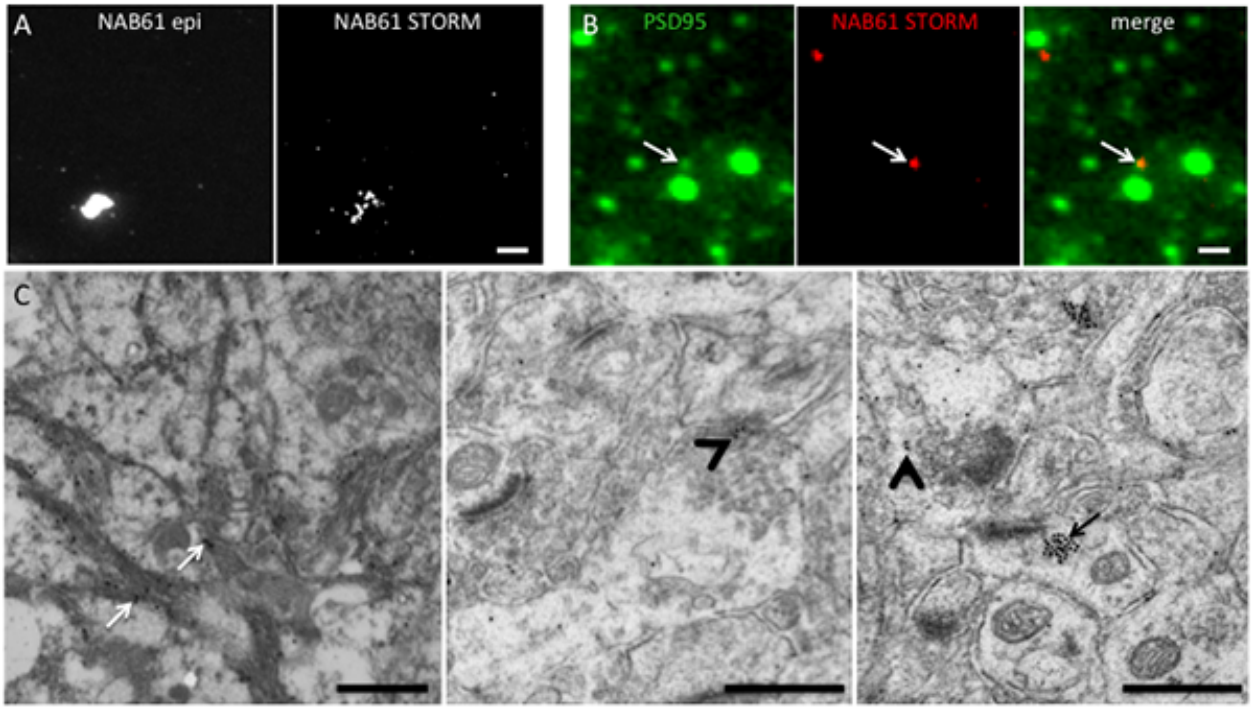

Figure 1. Confirmation of oAβ inside postsynaptic densities with STORM and TEM.

STORM imaging of oligomeric Aβ labeled with NAB61 (A) shows the increased resolution of STORM compared to epifluorescence (epi). Overlaying the NAB61 STORM image with PSD95 fluorescence (B) shows small oAβ punctae labeling synapses in the vicinity of plaques (arrow). Immunogold-TEM for NAB61 (C) shows 15 nm gold labeling of plaque fibrils (white arrows). NAB61 is also observed in a subset of postsynapses (black arrow) and presynaptic terminals (arrowheads). Filaments were not observed in the synapses labeled with NAB61 indicating that a non-filamentous form of Aβ is present at synapses. Scale bars represent 5 μm in A, 1 μm in B, and 500 nm in C.

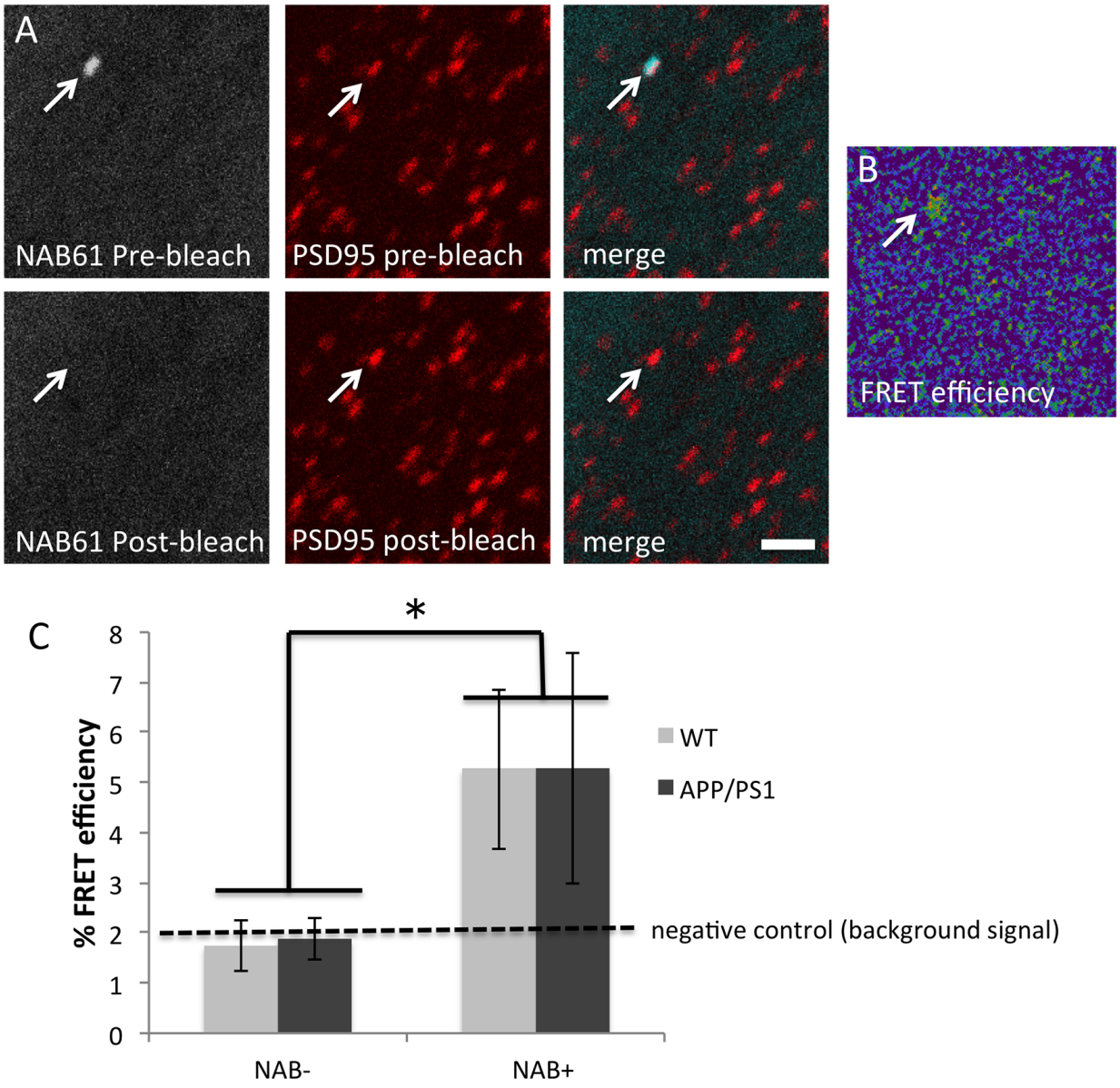

Figure 2. FRET analysis suggests that oAβ is present within the postsynaptic density.

FRET imaging was carried out on samples stained with PSD95 labeled with a Cy3 donor secondary antibody and NAB61 labeled with a Cy5 acceptor antibody. The intensity of the Cy3 labeling in synapses positive for NAB61 (arrow) increased after photobleaching the acceptor (A), indicating that NAB61 and PSD95 are within 10-30 nm of each other allowing non-radiative energy transfer between the donor and acceptor fluorophores before bleaching. The FRET efficiency, plotted with a color map where red and yellow represent higher FRET efficiency,

shows increased FRET in synapses positive for oAβ (arrow, B). Two-way ANOVA comparing NAB+ and NAB- synapses in APP/PS1 and wild-type mice reveal an increased FRET efficiency in NAB+ synapses indicating a close association between PSD95 and NAB61 (C). * $p<0.05$ ANOVA. Scale bar represents 2 μm.

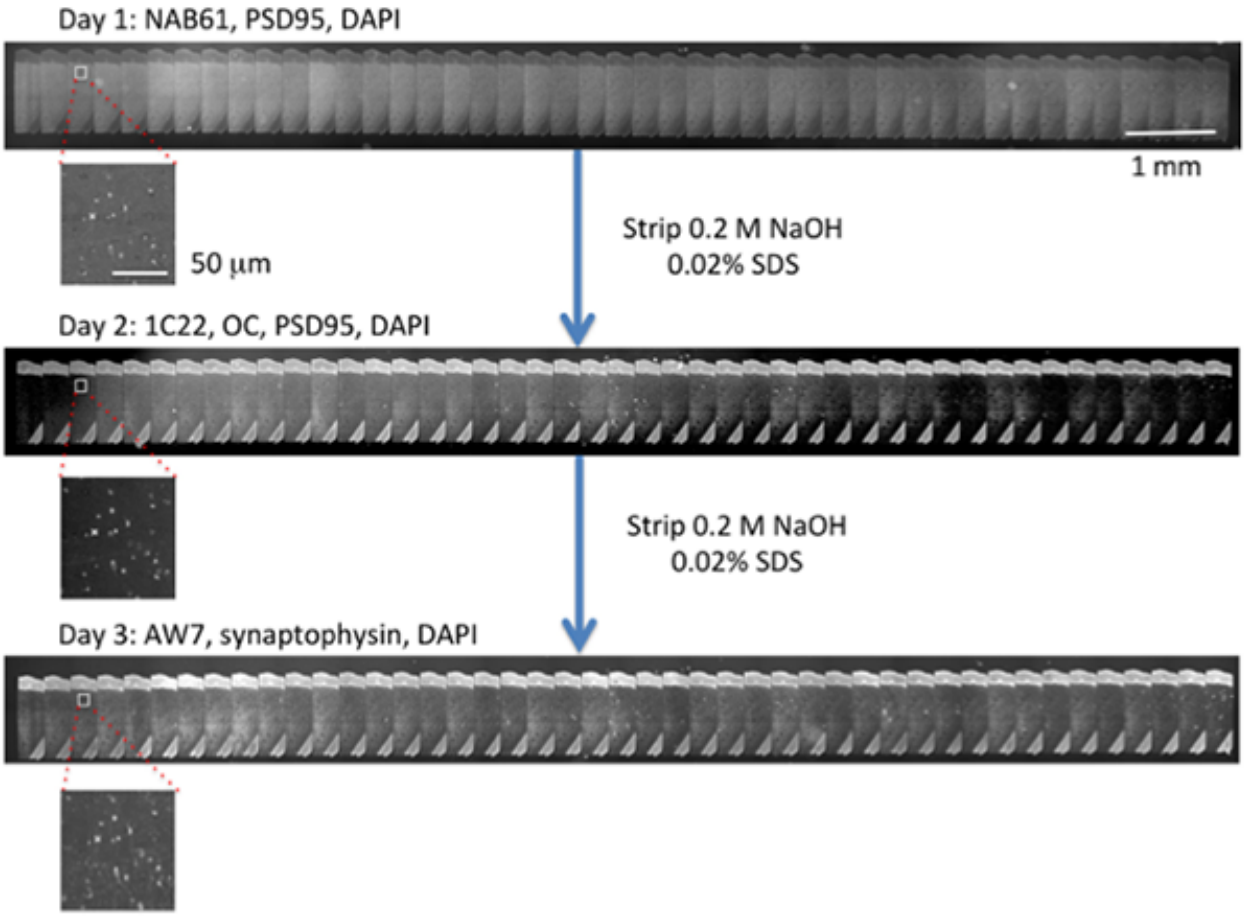

Figure 3. Array tomography experimental outline. Array tomography (three day process) was performed on ribbons of 70 nm thick sections of mouse brain tissue blocks in order to sequentially label oAβ and synaptic proteins as illustrated. A tilescan was acquired of the DAPI staining (grey) at 10x magnification along the entire ribbon. The nuclear pattern was used to ensure the same region was imaged each day and to allow alignment of stacks between days (insets).

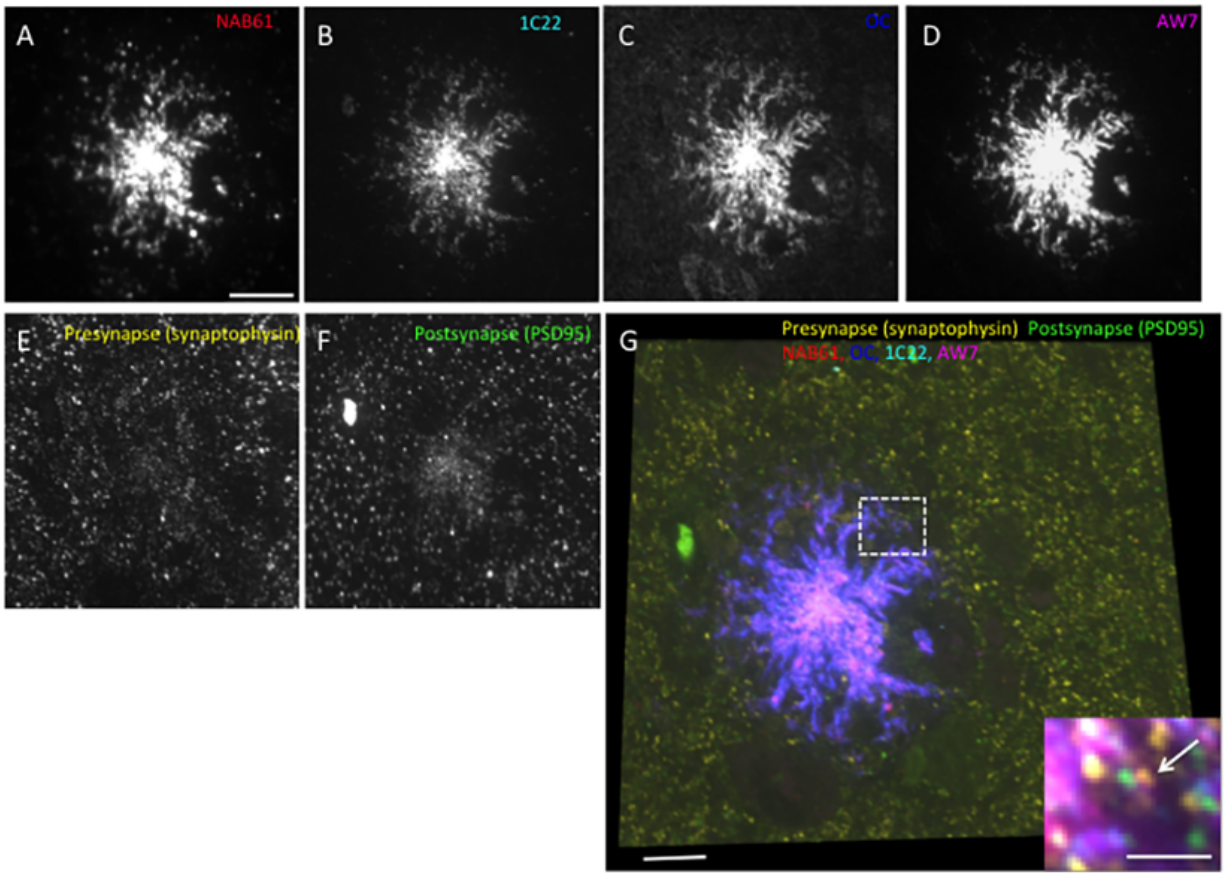

Figure 4. Array tomography staining of different anti-Aβ antibodies in brain tissue. NAB61 (A), 1C22 (B), OC (C) and AW7 (D) were used to label Aβ species, and synaptophysin (E) and PSD95 (F) were used to label pre- and post-synapses in APP/PS1 mouse tissue. A three-dimensional reconstruction of all merged channels is shown in (G) with inset (zoom in on dotted box) demonstrating the ability to resolve single synapses (arrow). Scale bars represent 10 μm in individual images and merged image (A-G) and 2 μm in the inset in (G).

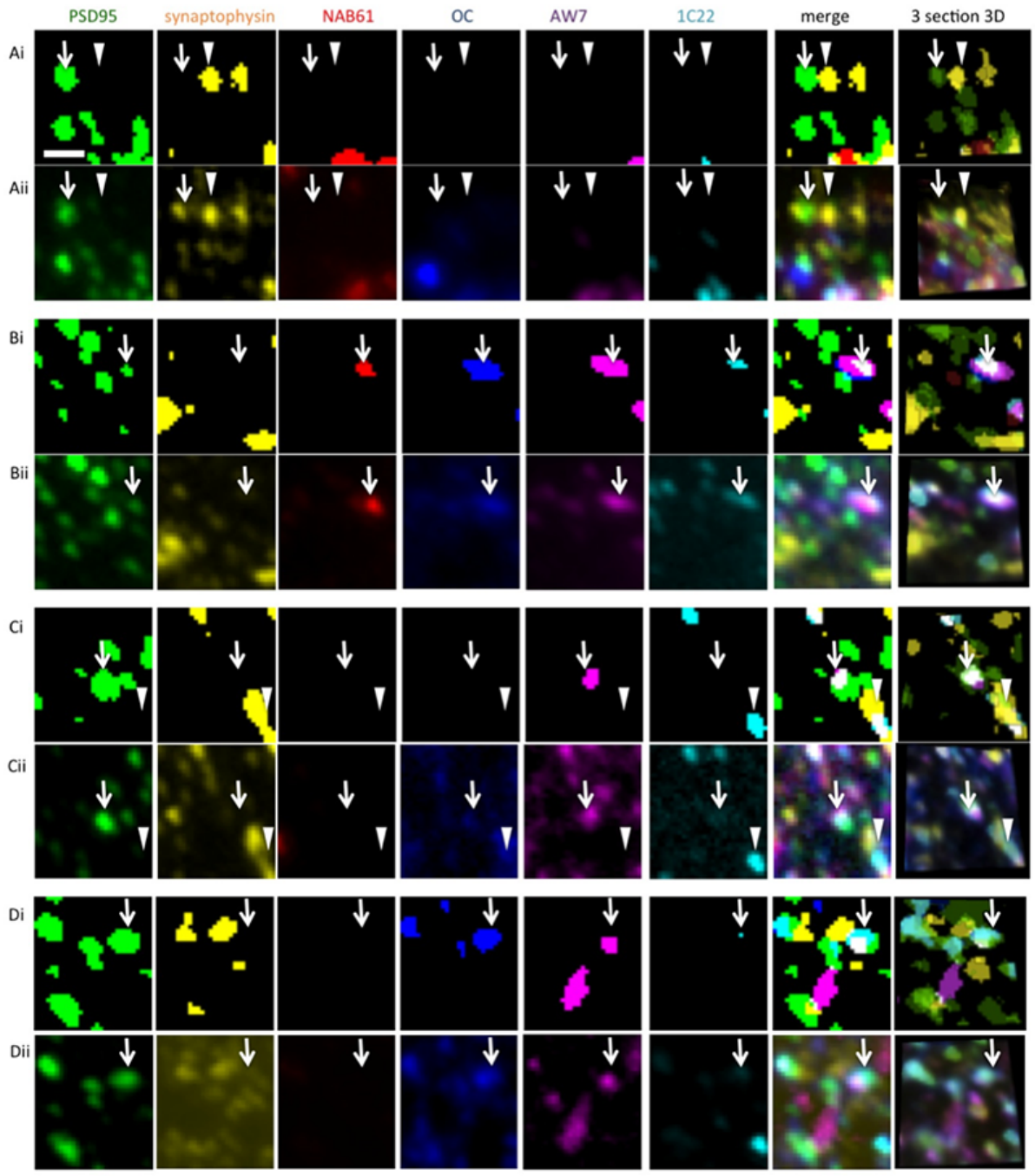

Figure 5. Array tomographic colocalization of anti-Aβ antibodies with pre- and post-synapses in APP/PS1 tissue. Examples of array tomography images that have been processed (thresholded, filtered for single-section objects, i) and raw (ii) array tomography images of APP/PS1 tissue showing the colocalization of Aβ detecting antibodies with pre-

(arrowheads) and post- (arrows) synapses. Left panels show single 70 nm thick sections and far right panels show a three-dimensional reconstruction of 3 consecutive serial sections. Panel A) shows pre and post-synaptic punctae without Aβ staining. B) shows a post-synapse labelled with all four tested Aβ antibodies. C) shows a pre-synapse labelled with 1C22 and a post-synapse labelled with AW7 and D) shows PSD staining colocalizing with OC, AW7, and 1C22. Scale bar represents 1 μm.

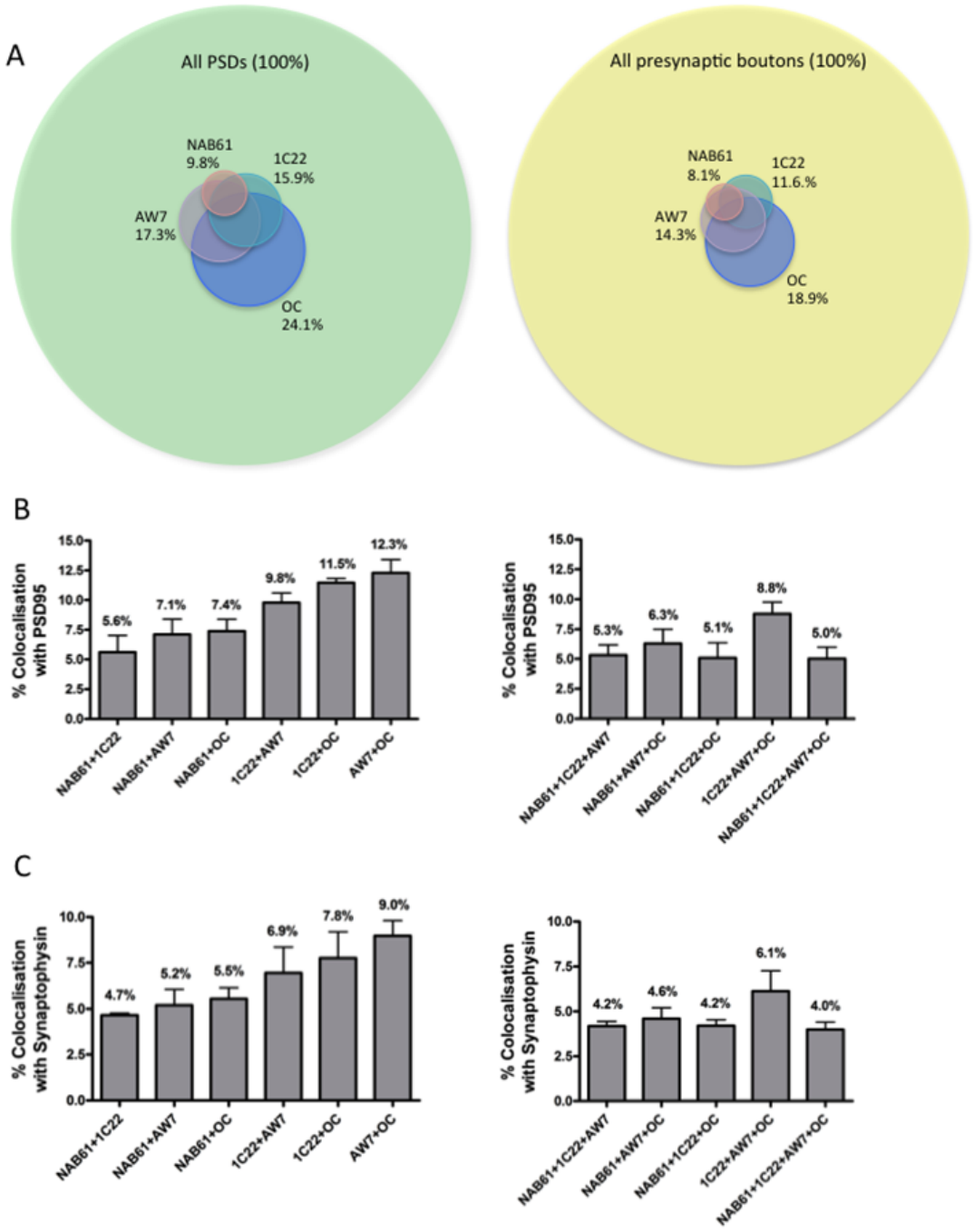

Figure 6. Multiple antibodies confirm the presence of oligomeric Aβ assemblies at pre- and post-synapses. Quantification of the three-day array tomography staining paradigm reveals partially overlapping populations of pre and postsynaptic terminals stained with the four anti-Aβ antibodies used. Venn diagrams (A) show the percentage of synapses stained with a single marker and approximate the overlap between the stains. The precise amount of co-

staining with each combination of antibodies is shown for post- (B) and pre-synaptic (C) terminals. Medians and interquartile ranges across all mice are shown.

Supplemental Figures:

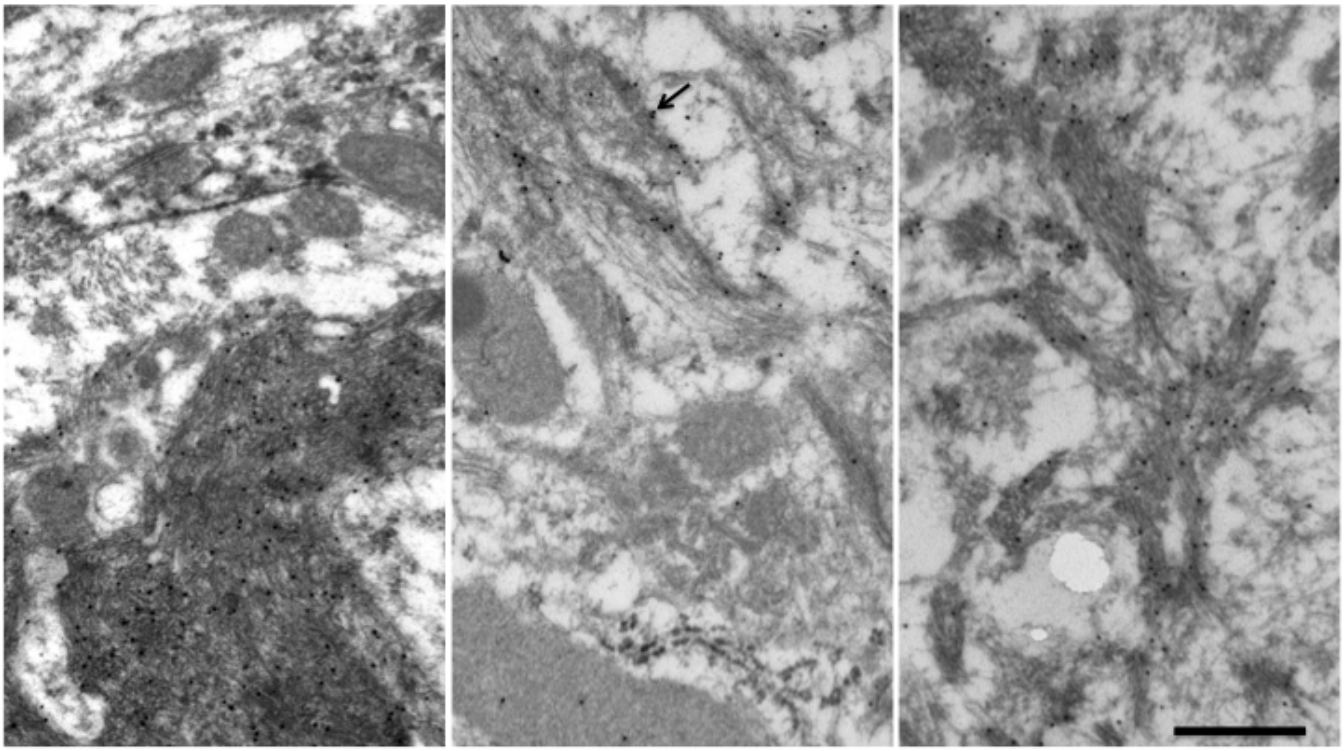

Supplemental Figure 1. Robust NAB61 staining around plaque fibrils. NAB61 immunogold labeling (black dots) is shown in association with plaque fibrils in APP/PS1 mouse brain. Arrow points to NAB61 staining at the PSD of a synapse. Scale bar represents 500 nm.

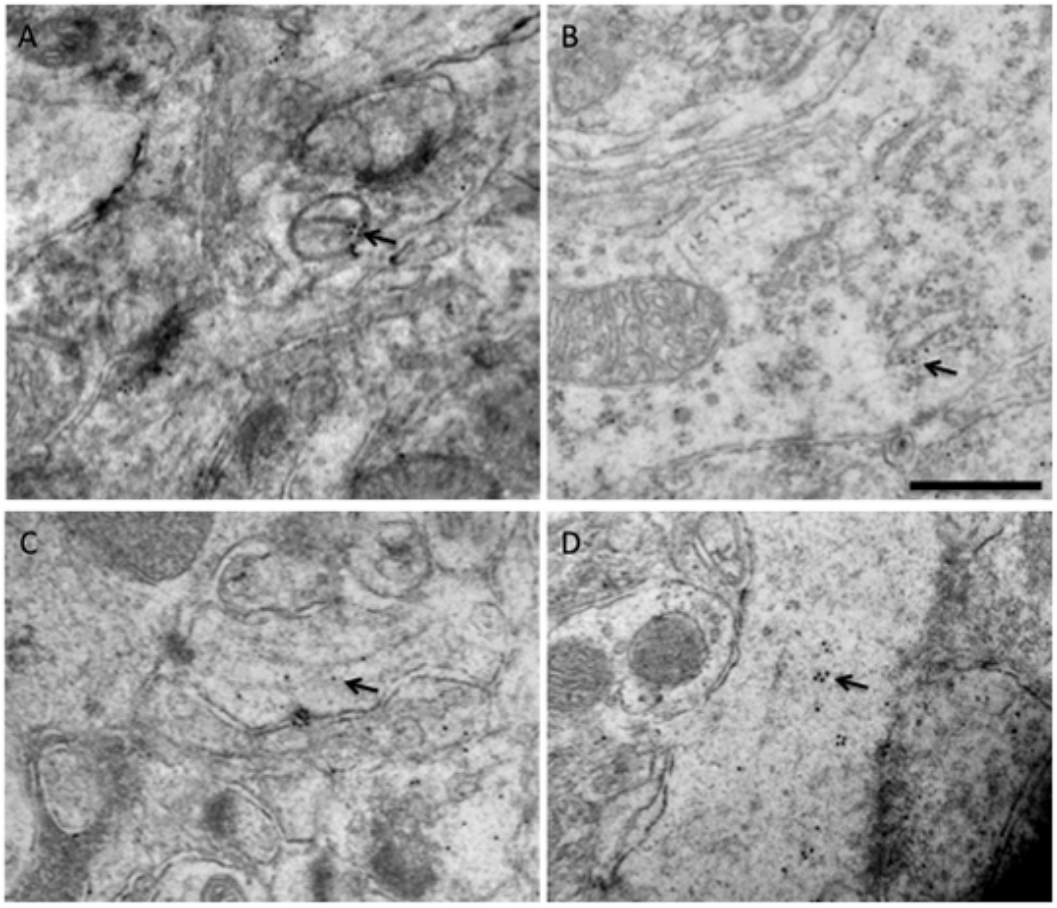

Supplemental Figure 2. Oligomeric Aβ staining was observed in structures other than plaques and synapses. Arrows show immunogold labeling of NAB61 in mitochondria (A), neuronal somatic cytoplasm associated with rough endoplasmic reticulum (B), and in dendrites (C and D). Scale bar represents 500 nm.

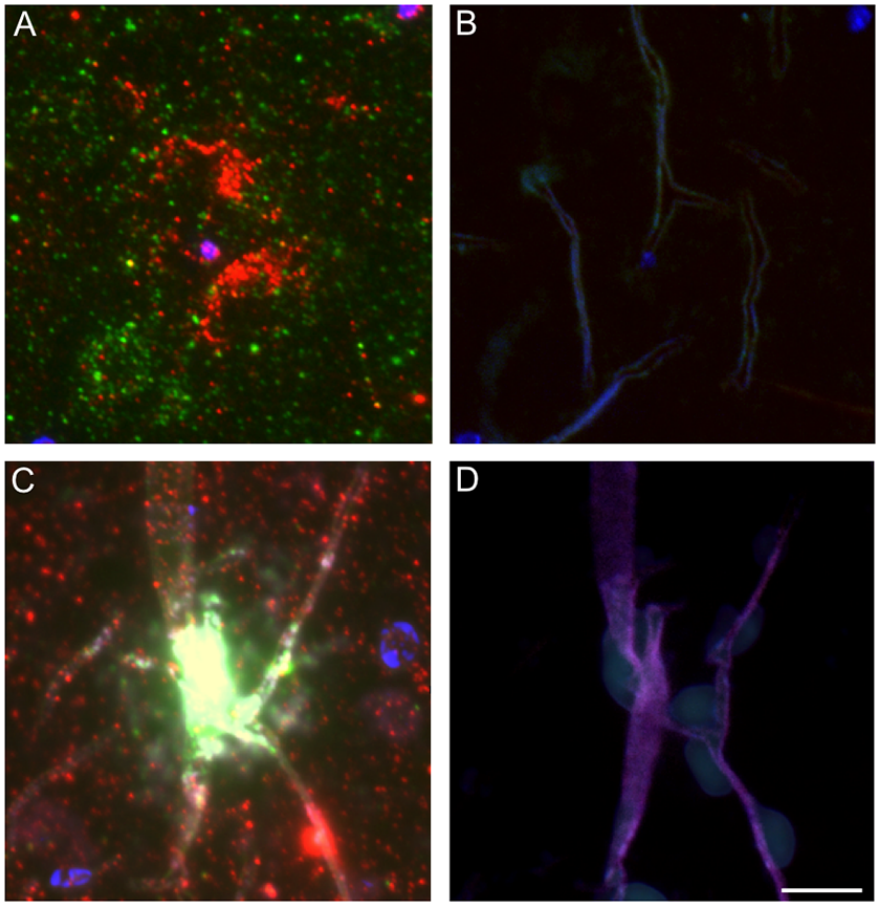

Supplemental Figure 3. Antibody stripping removes synaptic and plaque labeling. Short ribbons of sections were used to confirm stripping efficacy in each experiment. Panel A shows postsynaptic staining with PSD95 and plaque staining with NAB61 on day 1. Panel B is the same area of the section after stripping and re-probing with secondary antibody (no primary). Similarly plaque staining on Day 2 with 1C22 and OC and postsynaptic staining with PSD95 (Panel C) is completely absent after stripping and re-probing with secondary antibodies on Day 3 (Panel D). Scale bar represents 10 μm.